

## Conduction channels at finite bias in single-atom gold contacts

Mads Brandbyge

*Mikroelektronik Centret (MIC), Technical University of Denmark, Building 345E, DK-2800 Lyngby, Denmark*

Nobuhiko Kobayashi

*Surface and Interface Laboratory, The Institute of Physical and Chemical Research (RIKEN), 2-1 Hirosawa, Wako, Saitama 351-0198, Japan*

Masaru Tsukada

*Department of Physics, Graduate School of Science, University of Tokyo, 7-3-1 Hongo, Bunkyo-ku, Tokyo 113-0033, Japan*

(Received 8 June 1999; revised manuscript received 20 August 1999)

We consider the effect of a finite voltage bias on the conductance of single-atom gold contacts. We employ a nonorthogonal *spd*-tight-binding Hamiltonian combined with a local charge neutrality assumption. The conductance and charge distributions for finite bias are calculated using the nonequilibrium-Green-function formalism. We calculate the voltage drop through the contacts and find the main drop located near the negative electrode. We argue that this is due to the filled *d*-state resonances. The conduction is analyzed in terms of transmission eigenchannels and density of states of the eigenchannels projected onto tight-binding orbitals. We find a single almost fully transmitting channel with mainly *s* character for low bias while for high bias this channel becomes less transmitting and additional channels involving only *d* orbitals start to conduct. [S0163-1829(99)05447-8]

### I. INTRODUCTION

Manipulation of single-atom gold chains connected to bulk gold electrodes and measurements of their conductance has recently attracted much attention.<sup>1,2</sup> In experiments using superconducting electrodes it has been possible to extract transmissions of individual conductance channels for contacts down to the single atom.<sup>3</sup> The number of conduction channels and their relation to the valence of the atoms has been established in agreement with theory.<sup>3-7</sup> For one atom-wide gold contacts a single contributing channel is found in accordance with recent conductance fluctuation measurements<sup>8</sup> and the earlier interpretation of the  $G_0 = 2e^2/h$  peak in conductance histograms of ensembles of contacts.<sup>9</sup>

However, in the case of a *finite* voltage bias the behavior of the nonlinear conductance of these systems is not well understood. Yasuda and Sakai<sup>10</sup> found that the  $G_0$  peak in the conductance histogram of gold at room temperature disappeared gradually between approximately 1.5 and 2.0 V. On the other hand measurements of the *I-V* characteristics of these systems by Costa-Krämer and co-workers<sup>11</sup> show a highly nonlinear behavior already in the small bias regime ( $\sim 0.1$  V).

In this paper we consider chains of gold atoms connected to semi-infinite gold electrodes and calculate within a one-electron model transmissions and orbital components of the conductance channels at finite bias voltage. We use a nonorthogonal tight-binding model and employ the nonequilibrium Green-function approach combined with the assumption of local charge neutrality of the atoms.<sup>12,5</sup> The charge neutrality is fulfilled in a self-consistent manner *also* in the finite bias situation which enables us to determine the voltage drop along the contact.<sup>13</sup> We calculate the transmission eigen-

channel decomposition of both conductance and orbital projected density of states in order to determine the set of underlying conducting orbitals.

For the gold contacts, we find that the voltage drop preferentially occurs at the negative electrode. In the limit of zero bias we find a single contributing channel with almost perfect transmission consisting of orbitals ( $s, p_z, d_{z^2}$ ) with zero angular momentum in the direction of the contact ( $z$  direction hereafter) and with dominating *s* character. For a high-bias voltage of the order of 1.5 V we find that channels consisting of *d*-states ( $d_{zx}/d_{yz}$ ) with higher angular momenta ( $l_z=1$ ) come into play. The highly nonlinear experimental *I-V* characteristics seen by Costa-Krämer *et al.*<sup>11</sup> cannot be explained by our results.

The paper is organized as follows: First, we discuss how we include a nonorthogonal orbital basis in the calculation of electric current and in the implementation of atomic charge neutrality. This extends previous formulations,<sup>12,5,13,14</sup> which were based on a orthogonal orbital basis. Then we discuss how to analyze the total transmission and projected density of states in terms of transmission eigenchannels. After these formal sections we apply the formalism to specific examples of contacts containing a single atom chain. Finally, we discuss the obtained results in relation to experimental results.

### II. MODEL

Self-consistent *ab initio* methods<sup>15,7,16</sup> have been used to calculate the conductance of single atom contacts with *s-p* valence electrons (C,Na,Mg,Al,Si). The nonlinear conductance has been calculated by Lang for single atom Al and Al-Br contacts.<sup>17</sup> These computational methods are very demanding even for simple systems. In the case of transition metal contacts with quite localized *d*-states, simpler tight-

binding methods are therefore attractive despite their more approximative nature.<sup>14,5</sup>

We consider first the (spin-independent) *orthogonal* tight-binding Hamiltonian describing the left ( $|L\rangle$ ) and right ( $|R\rangle$ ) electrode states coupled via the contact region with  $N$  states ( $|\alpha\rangle$ ) by the matrix elements  $\mathbf{V}$ ,

$$\hat{H} = \sum_{LL'} \mathbf{h}_{LL'} |L\rangle \langle L'| + \sum_{RR'} \mathbf{h}_{RR'} |R\rangle \langle R'| + \sum_{\alpha\alpha'} \mathbf{H}_{\alpha\alpha'} |\alpha\rangle \langle \alpha'| + \left( \sum_{L\alpha} \mathbf{V}_{\alpha L} |\alpha\rangle \langle L| + \sum_{R\alpha} \mathbf{V}_{\alpha R} |\alpha\rangle \langle R| + \text{H.c.} \right). \quad (1)$$

Using the nonequilibrium-Green-function formalism (see, e.g., Refs. 13,18,19 and references therein) the electronic current through the contact can be derived for this model,

$$I(V) = G_0 \int_{-\infty}^{\infty} d\epsilon [n_F(\epsilon - eV/2)] - n_F(\epsilon + eV/2)$$

$$\text{Tr} \{ [\text{Im} \Sigma_L(\epsilon - eV/2)] \mathbf{G}^\dagger(\epsilon) [\text{Im} \Sigma_R(\epsilon + eV/2)] \mathbf{G}(\epsilon) \}. \quad (2)$$

Here,  $\mathbf{G}$  is the retarded Greens function ( $N \times N$ ) matrix  $\mathbf{1}/[\mathbf{1}(\epsilon + i\delta) - \mathbf{H} - \Sigma]$  for the finite contact region, and  $n_F$  is the Fermi function (we assume zero temperature throughout this paper). The self-energy,  $\Sigma = \Sigma_L + \Sigma_R$ , due to the coupling to the left and right electrodes is determined from the unperturbed ( $\mathbf{V}=0$ ) electrode Greens function  $\mathbf{g}^{(0)}$ ,

$$[\Sigma_L(\epsilon)]_{\alpha'\alpha} = \sum_{L,L'} \mathbf{V}_{\alpha'L'} [\mathbf{g}^{(0)}(\epsilon)]_{L'L} \mathbf{V}_{L\alpha}. \quad (3)$$

### A. Nonorthogonal tight-binding parameters

Parameters for tight-binding Hamiltonians can be determined by fitting to *ab initio* bandstructures obtained in density functional calculations. Here, we consider the case of gold and use a parametrization obtained by Mehl and Papaconstantopoulos, which is fitted to bulk gold systems.<sup>20</sup>

In general the most accurate parameter fits are obtained using a nonorthogonal tight-binding basis. It is straightforward to implement the overlap (overlap matrix  $\mathbf{S}_{ij} = \langle i|j\rangle$ ) between the states of the *separate* systems ( $\mathbf{S} = \mathbf{S}_L \oplus \mathbf{S}_\alpha \oplus \mathbf{S}_R$ ) by the Löwdin construction.<sup>21</sup> In terms of the matrix elements  $\mathbf{M}_O \in \{\mathbf{h}_O, \mathbf{H}_O, \mathbf{V}_O\}$  in Eq. (1) corresponding to the orthogonal basis, the matrix elements  $\mathbf{M}$  corresponding to the nonorthogonal basis read,<sup>22</sup>

$$\mathbf{M} = \mathbf{S}^{1/2} \mathbf{M}_O \mathbf{S}^{1/2}. \quad (4)$$

Inserting  $\mathbf{1} = \mathbf{S}^{-1/2} \mathbf{S}^{1/2}$  in the formula for the current, Eq. (2), this procedure simply amounts to replacing orthogonal parameters ( $\mathbf{M}_O$ ) by nonorthogonal ones ( $\mathbf{M}$ ) and substituting  $\epsilon$  by  $\epsilon \mathbf{S}$  in all Greens-function matrices in Eqs. (2) and (3).

The remaining overlap between the states in the finite contact region and electrodes (we assume that the left and right electrode states have no overlap) can be included via a redefinition of the hopping matrix elements, as shown recently by Emberly and Kirczenow,<sup>23</sup>

$$\mathbf{V}_{\alpha L(R)} \rightarrow \mathbf{V}_{\alpha L(R)} - \epsilon \mathbf{S}_{\alpha L(R)}. \quad (5)$$

### B. Self-consistent screening at finite bias

In equilibrium (no current,  $V=0$ ) the number of valence electrons associated with an atomic site  $i$  (with orbitals  $\alpha_i$ ) can be found from the retarded Greens function,

$$Q_i = -\frac{2}{\pi} \int_{-\infty}^{\infty} d\epsilon \sum_{\alpha_i} \text{Im}[\mathbf{S}\mathbf{G}(\epsilon)]_{\alpha_i\alpha_i} n_F(\epsilon). \quad (6)$$

Strictly speaking we should use  $\mathbf{S}^{1/2} \mathbf{G} \mathbf{S}^{1/2}$  instead of the simpler  $\mathbf{S}\mathbf{G}$  in this formula, but the results are equal to first order in  $\delta \mathbf{S} \equiv \mathbf{S} - \mathbf{1}$ , and the total number of electrons in all orbitals remain exactly the same.

While the number of valence electrons for the atoms well inside the bulk corresponds to  $Z=11$ , the low-coordinated atoms in the contact region will in general not be charge neutral. Following Refs. 12 and 5 we assume charge neutrality of each atom in the contact region and adjust the local potential at each atom self consistently to achieve this.<sup>24</sup> The local potential corresponds to a diagonal matrix ( $\Phi_O = \text{diag}\{\phi_i\}$ ) added to the orthogonal Hamiltonian describing the contact. To first order in  $\delta \mathbf{S}$  the nonorthogonal matrix elements read,

$$\Phi_{ij} = (\mathbf{S}^{1/2} \Phi_O \mathbf{S}^{1/2})_{ij} \approx \mathbf{S}_{ij} (\phi_i + \phi_j)/2. \quad (7)$$

This expression ensures that a constant on-site shift of all states amounts to the same shift in all eigenenergies.

In the nonequilibrium case the chemical potentials well inside the left and right bulk electrodes differ by  $eV$ , and the charge can be written<sup>13,19</sup>

$$Q_i = -\frac{2}{\pi} \int_{-\infty}^{\infty} d\epsilon \sum_{\alpha_i} \times \{ [\mathbf{S}\mathbf{G}(\epsilon) \text{Im} \Sigma_L(\epsilon - eV/2) \mathbf{G}^\dagger(\epsilon)]_{\alpha_i\alpha_i} n_F(\epsilon - eV/2) + [\mathbf{S}\mathbf{G}(\epsilon) \text{Im} \Sigma_R(\epsilon + eV/2) \mathbf{G}^\dagger(\epsilon)]_{\alpha_i\alpha_i} n_F(\epsilon + eV/2) \}. \quad (8)$$

From the relation  $\text{Im} \mathbf{G} = \mathbf{G}(\text{Im} \Sigma) \mathbf{G}^\dagger$  it is easy to see that this reduces to the equilibrium expression in Eq. (6) for  $V=0$ . We solve the set of equations  $Q_i[\Phi] = Z$  ( $i=1, \dots, N$ ) self-consistently and thereby include the effect of a local potential change in the contact due to the finite bias. This method has been applied by Pernas, Martín-Rodero, and Flores.<sup>13</sup> They considered chains connected to electrodes (Bethe lattices) using a orthogonal tight-binding model with a single orbital per site. We will later return to their results.

In order to go beyond the charge neutrality approximation we should solve Poisson's equation to obtain the electrostatic potential as discussed by McLennan, Lee, and Datta<sup>18</sup> in the context of two-dimensional device models based on the nonequilibrium Green's-function formalism.

### III. EIGENCHANNEL ANALYSIS

The expression for the current, Eq. (2), can be written in the Landauer-Büttiker form,<sup>25</sup>

$$I(V) = G_0 \int_{-\infty}^{\infty} d\epsilon [n_F(\epsilon - eV/2) - n_F(\epsilon + eV/2)] \times \text{Tr}[\mathbf{t}^\dagger(\epsilon)\mathbf{t}(\epsilon)], \quad (9)$$

with the identification<sup>5</sup> of the (left-to-right) transmission amplitude matrix  $\mathbf{t}$ ,

$$\mathbf{t}(\epsilon) = \left[ \text{Im} \Sigma_R \left( \epsilon + \frac{eV}{2} \right) \right]^{1/2} \mathbf{G}(\epsilon) \left[ \text{Im} \Sigma_L \left( \epsilon - \frac{eV}{2} \right) \right]^{1/2}. \quad (10)$$

The transmission *eigenchannels* provide a direct picture of the electronic states that contribute to the conductance.<sup>4,5,7</sup> The eigenchannels are defined in terms of the (left to right) transmission matrix,<sup>26</sup>

$$\mathbf{t} = \mathbf{U}_R \text{diag}\{|\tau_n|\}\mathbf{U}_L^\dagger. \quad (11)$$

They split the total conductance into individual contributions,

$$G = G_0 \sum_n |\tau_n|^2. \quad (12)$$

The eigenchannel transmissions,  $|\tau_n|^2$ , are the eigenvalues of  $\mathbf{t}^\dagger \mathbf{t}$ .

### Projected density of states

The local density of states (not including bound states) can be split into a sum of eigenchannel components. The individual components can be calculated from the functional derivative of the transmission matrix with respect to the local potential  $V(\vec{r})$ ,<sup>27</sup>

$$\rho(\vec{r}, \epsilon) = -\frac{2}{\pi} \sum_n \text{Im} \left[ \mathbf{U}_L^\dagger \mathbf{t}^\dagger \frac{\delta \mathbf{t}}{\delta V(\vec{r})} \mathbf{U}_L \right]_{nn} / |\tau_n|^2. \quad (13)$$

A factor of 2 for spin has been included.

In the tight-binding formulation it is instead relevant to calculate the density of states of the individual eigenchannels projected onto selected orbitals (PDOS). Following Refs. 28 and 27 the tight-binding analog of Eq. (13) can be obtained by simply exchanging the  $V$ -derivative with the derivative with respect to the on-site element of the Hamiltonian  $\epsilon_\alpha$ , corresponding to orbital  $\alpha$ ,

$$\rho_\alpha(\epsilon) = -\frac{2}{\pi} \sum_n \text{Im} \left( \mathbf{U}_L^\dagger \mathbf{t}^\dagger \frac{\delta \mathbf{t}}{\delta \epsilon_\alpha} \mathbf{U}_L \right)_{nn} / |\tau_n|^2. \quad (14)$$

However, in the present case where the Greens function is known, a more direct formula can be derived by defining the matrix  $\mathbf{X}$ , which diagonalize the matrix inside the trace in Eq. (2),

$$\mathbf{X}^{-1} [(\text{Im} \Sigma_L) \mathbf{G}^\dagger (\text{Im} \Sigma_R) \mathbf{G}] \mathbf{X} = \text{diag}\{|\tau_n|^2\}. \quad (15)$$

Using the relation between  $\mathbf{t}$  and  $\mathbf{G}$  [Eq. (10)] in Eq. (14), and

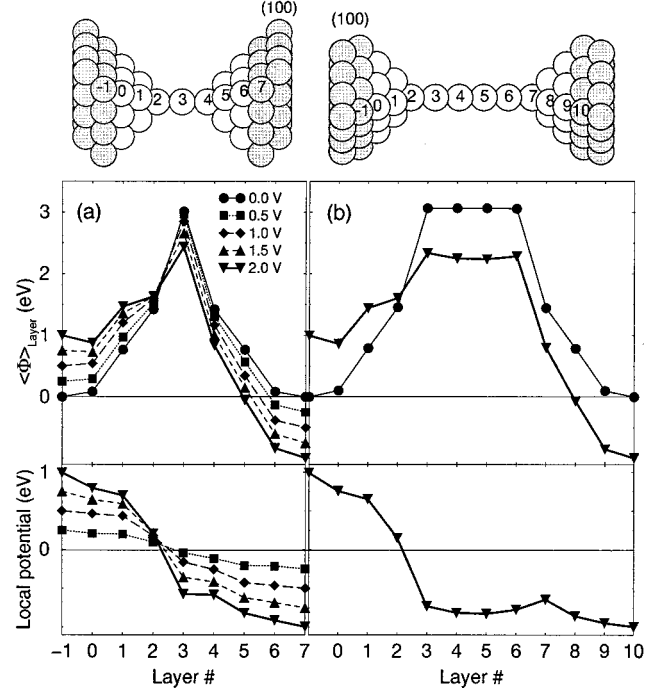


FIG. 1. The layer averaged atomic potential shifts ( $\langle \phi_i \rangle_{\text{Layer}}$ ) for different bias voltages for the chains of length 3 (a) and 6 (b). Layer  $-1$  corresponds to the first (100) surface layer of the semi-infinite electrode. Below the change in local potential (voltage drop) [ $\langle \phi_i \rangle_{\text{Layer}}(V) - \langle \phi_i \rangle_{\text{Layer}}(0)$ ] is shown. The largest voltage drop is seen close to the negative electrode (left) between layer 2 and 3 for both (a) and (b).

$$\frac{\partial \mathbf{G}}{\partial \epsilon_\alpha} = \mathbf{G} \mathbf{P}_\alpha \mathbf{G}, \quad (16)$$

where  $\mathbf{P}_\alpha$  is the matrix projecting onto orbital  $\alpha$ , we get the following formula for the PDOS split into eigenchannel components:

$$\rho_\alpha(\epsilon) = -\frac{2}{\pi} \sum_n \text{Im} [\mathbf{X}^{-1} \mathbf{P}_\alpha \mathbf{G} \mathbf{X}]_{nn}. \quad (17)$$

We will use the nonorthogonal tight-binding orbitals centered on a central atom in the contact region in the projection.

## IV. CALCULATIONS

We limit our study to a few simple contact geometries which contain an atomic chain in order to extract some general features. In these structures all interatomic distances are taken to be equal to the bulk distance. We would probably have to use tight-binding parameters fitted to *ab initio* calculations of the specific systems if we were to focus in on the detailed behavior for small variations in the geometry—e.g., changes in bond lengths and bond angles in the atomic chain. This is outside the scope of the present paper. In the calculations we first consider the two structures depicted in Fig. 1. They consist of a chain of 3 or 6 gold atoms attached to layers of 4 and 9 atoms in both ends which again are con-

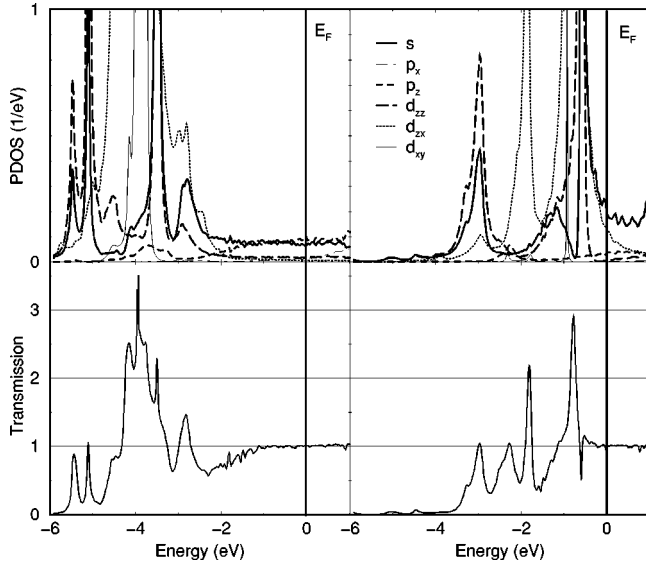


FIG. 2. The density of states projected onto the orbitals of the middle atom of the 3-atom chain ( $z$  is along the chain, contributions from the almost  $x \leftrightarrow y$  symmetric states are included in the curves labeled by  $p_x$ ,  $d_{zx}$ , and  $d_{xy}$ ) and the corresponding transmission vs energy. The bulk electrode Fermi energy is at zero. Left (right): Without (with) the self-consistent on-site potential.

nected to the (100) faces of two perfect semi-infinite gold electrodes.

The electrode Greens functions in Eq. (3),  $\mathbf{g}^{(0)}$ , are constructed from the solutions of the bulk eigenstates using the ideal construction e.g. described in Ref. 29. This implies that the on-site (relative to the bulk electrode chemical potential) and hopping terms of the semi-infinite electrodes are fixed at bulk values for all electrode atoms (gray in Fig. 1). For finite bias the chemical potential of an electrode is shifted and so the on-site term of the electrode atoms is shifted accordingly with the same amount. For the atoms in the contact region (white in Fig. 1) the (layer averaged) potential shifts calculated self-consistently for different bias voltages are shown in Fig. 1.

In Fig. 2 we show the density of states projected onto the orbitals of the middle atom in the 3-atom chain with (left panel) and without (right panel) the self-consistent potential. In both cases the presence of the  $d$  states is reflected in the transmission vs. incident electron energy. We note that the inclusion of the self-consistent potential shifts the  $d$  states closer to the Fermi level, and the  $d$  state PDOS shows more narrow features since these states are being shifted out of resonance with the  $d$  states on the contacting atoms. Around  $E_F$  a significant  $d$  component is present in the self-consistent case together with the  $s/p_z$  component whereas the  $s$  and  $p_z$  components dominate around the bulk electrode  $E_F$  in the non-self-consistent case. Both results yield a conductance plateau at  $G_0$  around  $E_F$ .

In Fig. 3 we show the eigenchannel transmissions for the self-consistent calculation of the 3-atom chain. At zero voltage a single eigenchannel is almost fully transmitting around  $E_F$  while the remaining eigenchannels have transmissions of 0.005 or less in accordance with Ref. 8. For a finite bias the states in an energy window (vertical lines) of width  $eV$  con-

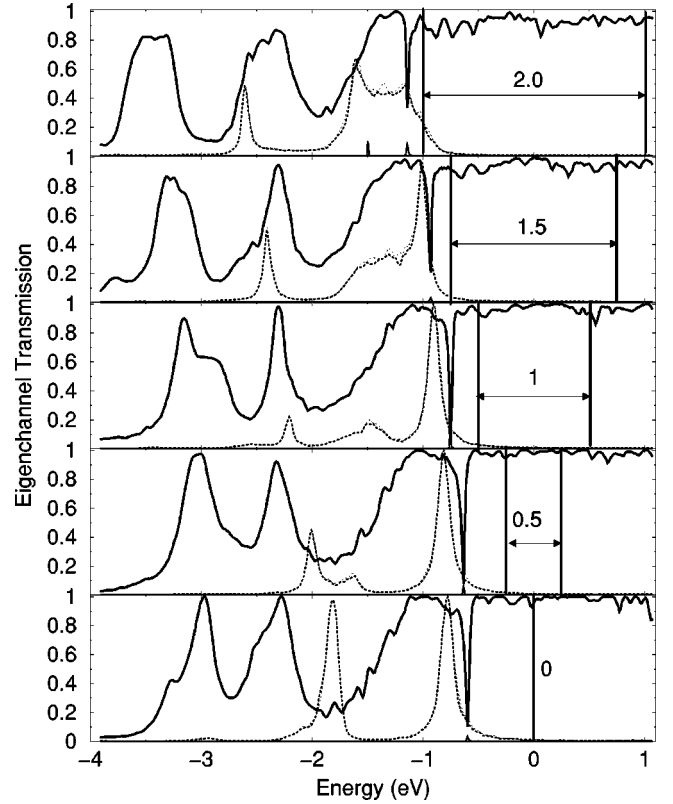


FIG. 3. The eigenchannel transmissions,  $|\tau_n|^2$ , of the 3-atom chain for different voltage bias,  $eV=0,0.5,1.0,1.5,2.0$ . An almost fully transmitting single-channel (solid line) is seen inside the voltage window and two near degenerate channels are seen just below (dotted lines) for 0 V (bottom panel). For higher bias voltages these degenerate channels begin to enter the voltage window. Very small peaks are just resolved corresponding to a 4th channel—the remaining eigenvalues are vanishing (0.005).

tributes to the current. The PDOS (cf. Fig. 2) resolved into its eigenchannel components using Eq. (17) for the first 3 channels is presented in Fig. 4 for 0 Volt and 2 Volt. From Figs. 3 and 4 it is seen that the  $d_{zx}/d_{yz}$ -derived channels first begin to contribute inside the voltage window from a voltage bias of about 1.5 V.

In Fig. 4 a peak is seen at the upper edge of the  $d_{z^2}$ -PDOS, which is followed by a peak in the  $s$ -PDOS with a decaying tail towards higher energies. At this point in Fig. 3 the first eigenchannel has a dip where a 4th channel contribution can just be resolved. Except for this the  $s$ ,  $p_z$ , and  $d_{z^2}$  orbitals combine into a single eigenchannel. A very narrow peak in PDOS is seen in Fig. 2 corresponding to the  $d_{xy}/d_{x^2-y^2}$  orbitals, but the corresponding resonant tunneling peaks are not seen in Fig. 3.

We have also considered shorter and longer chains. In contrast to the result for the 3 atom long chain we find for a 2 atom long chain that the  $p_x/p_y$  orbitals play a more pronounced role in the 2nd and 3rd eigenchannels and the model predict a noticeable contribution from the 2nd and 3rd eigenchannels of about 0.05 around  $E_F$ .

Formation of longer chains of gold atoms has been predicted by molecular-dynamics simulation (see, e.g., Ref. 30 for a chain with 6 atoms) and seen experimentally at low temperature for chains containing 4 or 5 atoms.<sup>1,2</sup> For the

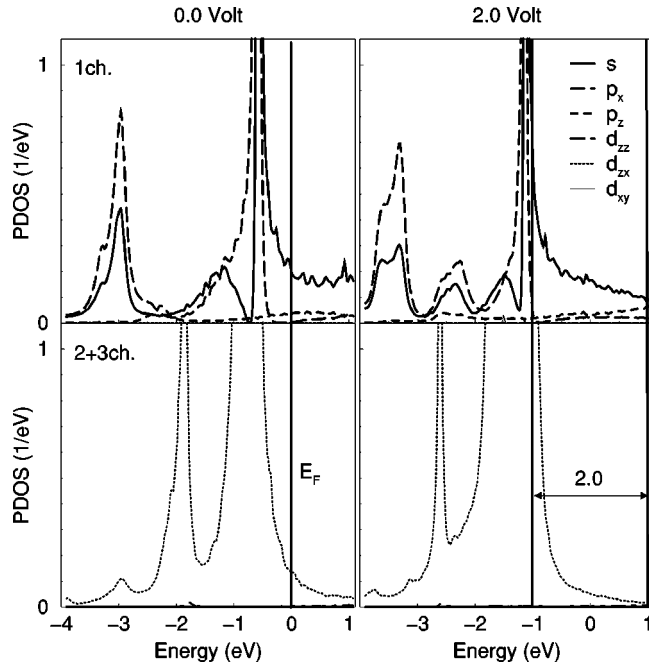


FIG. 4. The orbital projected DOS (corresponding to Fig. 2) for the first eigenchannel (upper) and the total of the almost degenerate 2nd and 3rd channels (lower) for 0 V (left panel) and 2 V (right panel).

chain of 6 atoms depicted in Fig. 1, we find that the upper edge of the  $d$ -band contributions gets quite close to  $E_F$ . This is expected already from the bandstructure of the infinite chain (Fig. 6) where the upper edge of the  $d_{zx}/d_{yz}$  bands are just cutting  $E_F$ . The correspondence between onset of channels in Fig. 5 at zero V and onset of bands in Fig. 6 is clear except for the very narrow  $d_{xy}/d_{x^2-y^2}$  bands.

Finally, we have considered a contact consisting of a 3 atom long chain attached to layers of 3 and 7 atoms in both ends which again are connected to the (111) faces of two perfect semi-infinite electrodes (see Fig. 7). For zero bias we find again a single almost fully transmitting channel [Fig. 7(a)] but the high transmission is only maintained in a rather narrow energy window around  $E_F$  in contrast to the (100) results. A single-atom gold contact in the (111) direction has also been considered by Cuevas *et al.*<sup>6</sup> in the case of zero bias. They also found that the channel transmission peaked close to  $E_F$  with almost full transmission. However in that study the  $d$  electrons were neglected. For high bias [Fig.

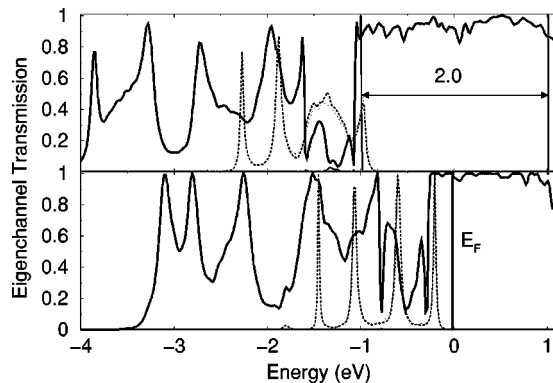


FIG. 5. Eigenchannel transmissions for the 6 atom chain.

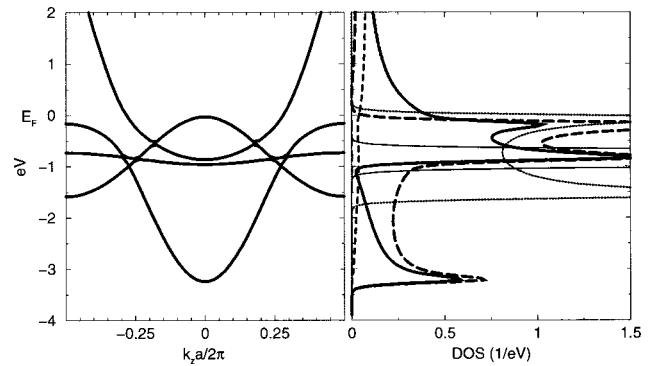


FIG. 6. The band-structure and orbital DOS for the infinite gold chain with bulk interatomic distance. A finite broadening is used in the DOS figure. The different line types refer to the orbitals as in Figs. 2 and 4.

7(b)] we find a considerable decrease in  $I/V$  compared to the (100) result ( $\sim 30\%$ ).

### Voltage drop

We note that the potential shift shown in Fig. 1(b) for the 6 atom chain is almost constant along the four middle atoms. The change in local potential (voltage drop) takes place mainly in the first part of the chain between the first two atoms (2-3) and in the entrance in-between the first layer (1) and the first atom (2). This is also the case for the 3-atom chains connected to the (100) or (111) electrodes.

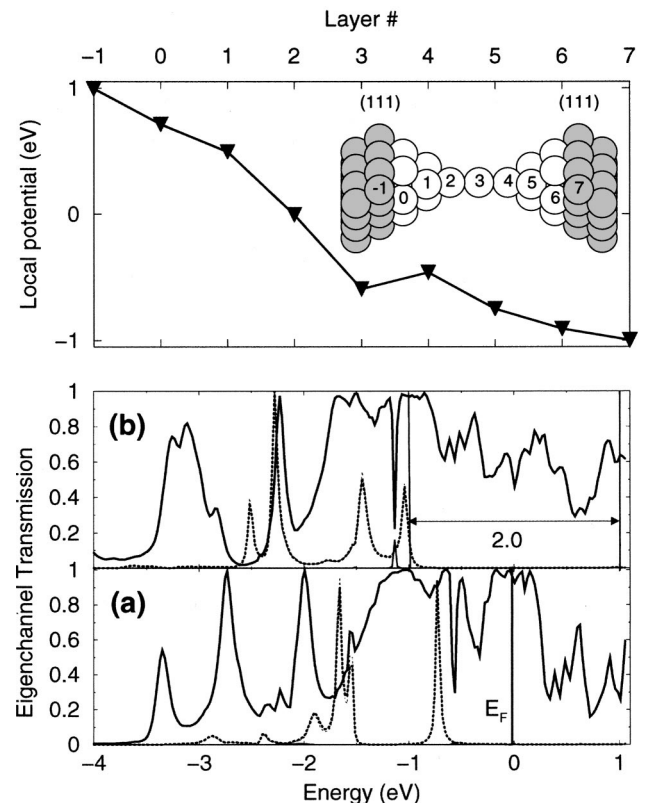


FIG. 7. The voltage drop for 2 V bias in a 3 atom contact connected to (111) electrodes (upper panel). Below we show the eigenchannel transmissions for (a) 0-V and (b) 2-V bias.

The calculated voltage drop has no symmetry despite the left-right symmetry of the gold contacts. The main voltage drop is located near the the negative electrode (left Figs. 1 and 7). This is in contrast to the calculations by Pernas *et al.*<sup>13</sup> for the symmetric *s*-orbital chains connected to Bethe lattices, which yield a left-right antisymmetric voltage drop. An explanation for this can be found in the difference in electronic structure: The system examined by Pernas and coworkers<sup>13</sup> has besides the left-right symmetry also electron-hole symmetry which implies (cf. Eq. 8) that the local potential,  $\Phi(V)$ , becomes an odd function of  $V$ . For a left-right symmetric contact the voltage drop will therefore be left-right antisymmetric. However, in general there will be an asymmetry in the DOS or in the orbital filling of the system and thus we cannot expect a symmetric voltage drop from Eq. (8). For example, electrodes with fcc or bcc lattice will not have a symmetric DOS around its Fermi energy.

It is instructive to consider the case of a single contact state at energy  $\varepsilon_0$  (with respect to  $E_F=0$ ) connected to wide band electrodes in a symmetric way:  $\Sigma_{L/R}(\varepsilon)=i\Gamma$ . In this case Eq. 8 yields a relation for the on-site energy  $\varepsilon_0(V)$ ,

$$\arctan\left[\frac{\varepsilon_0(V)+(eV/2)}{2\Gamma}\right] + \arctan\left[\frac{\varepsilon_0(V)-(eV/2)}{2\Gamma}\right] = 2 \arctan\left[\frac{\varepsilon_0(0)}{2\Gamma}\right]. \quad (18)$$

It can be seen from this that a half-filled resonance,  $\varepsilon_0(0)=0$ , will keep this value for finite bias. On the other hand, a resonance with higher filling [ $\varepsilon_0(0)<0$ ] will lower its on-site energy further for finite bias to compensate depopulation. The voltage drop between the resonance and the negative electrode will therefore be larger than the voltage drop between the resonance and the positive electrode. For a less than half filled resonance the situation is reversed. This is illustrated in Fig. 8.

For the gold contacts the DOS shown in Fig. 2 displays large resonance features at the upper edge of the *d*-state contributions just below the Fermi energy. Above the Fermi energy the DOS is more smooth. We can understand why the main voltage drop takes place at the negative electrode for high bias from the simple argument above. For low bias [0.5 eV in Fig. 1(a)] where the resonance peaks are not entering the voltage window we find a almost left-right antisymmetric voltage drop.

## V. DISCUSSION

The transmission functions presented in Figs. 3, 5, and 7 change significantly with increased bias: The local charge neutrality forces the  $d_{zx}/d_{yz}$  states down in energy and delays the onset of the derived eigenchannels. The transmission of the  $s/p_z/d_{z^2}$  ( $l_z=0$ ) channel within the voltage window is lowered with increasing bias. The partially open  $d_{zx}/d_{yz}$  transmission channels as well as the lowering of the  $s/p_z/d_{z^2}$  transmission in the high bias regime lead to an increased electron-ion momentum transfer (electron wind) where the current carrying electrons are backscattered. The backscattering takes place mainly between the first two atoms in the entrance of the chain according to the voltage drop in Fig. 1. An increased electron wind could be part of the reason for

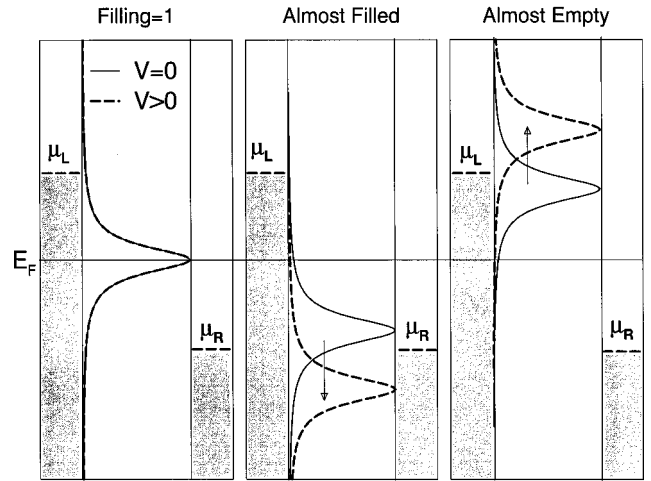


FIG. 8. A single state coupled to the left and right electrodes with equal and constant coupling. For the half-filled resonance the charge will not change with bias and thus the resonance energy remain fixed. The local potential shift will decrease (increase) the resonance energy with bias for the almost filled (empty) resonance in order to fix its charge.

the apparent gradual destabilization of the one-atom contacts between 1.5 and 2.0 V observed by Yasuda and Sakai.<sup>10</sup> In accordance with this, long chains was reported to be stable for a bias of 1 V in Ref. 2.

The large increase in conductance found in Ref. 11 is not seen in the results in the present paper. In contrast to this we find that the increased bias will cause a small [(100) electrodes] or moderate [(111) electrodes] decrease in the conductance. We should keep in mind, however, that tunneling currents through the vacuum gap between the electrodes is not included in the present calculation and could contribute in a significant way.<sup>31</sup>

For the long chains, the *d*-derived electronic states inside the chain will approach the one-dimensional band states with the sharp onset in the corresponding transmission channels close to Fermi energy cf. Figs. 5 and 6. In the calculation the strict local charge neutrality forces the *d* states down in energy with increased bias preventing nonlinearity due to these states. In a more relaxed description of screening one can imagine that the *d* states may enter already in the small bias voltage regime and could lead to some nonlinearity for the chain with 6 or more atoms, but for the 3 atom chain this does not seem possible.

On the other hand, electron-electron interaction beyond the simple charge neutrality used in the present paper may play a role for long ordered chains. It can also be relevant in the ‘‘coupled quantum dot’’ limit of large atomic separation in the chain. Large atomic separations in gold chains have been suggested by some experiments.<sup>1,2</sup> However the apparent stability of these chains are in contrast to density functional simulations.<sup>32</sup> Jonson *et al.*<sup>33</sup> have suggested a Luttinger liquidlike effect as an explanation of the observed low bias nonlinearity in Ref. 11. Kawahito *et al.*<sup>34</sup> have calculated the conductance for an *s*-state tight-binding model including a local Hubbard term at zero bias. It would be of interest to include a Hubbard interaction in the present type of calculation in order to elucidate the role of electron-electron interactions further.

In conclusion, we have calculated the finite bias conductance of single-atom gold contacts within a local charge neutral tight-binding model. We find that the voltage drop takes place mainly near the negative electrode and attribute this to the  $d$ -state resonances just below the Fermi energy. We have analyzed the results in terms of transmission eigenchannels. At low bias voltage a single free electronlike channel consisting of  $l_z=0$  states ( $s, p_z$ , and  $d_{z^2}$ ) is conducting. For high-bias voltage pure  $d$  state channels with  $l_z=1$  ( $d_{xz}/d_{yz}$ ) begin to contribute to the conductance.

## ACKNOWLEDGMENTS

The authors thank M. Mehl for helpful communications, and A-P. Jauho and N. A. Mortensen for useful comments on the manuscript. Discussions with S. R. Bahn, K. Hansen, K. W. Jacobsen, H. Nakanishi, and K. Stokbro are gratefully acknowledged. This work has been supported by the Core Research for Evolutional Science and Technology (CREST) of the Japan Science and Technology Corporation (JST) and the Danish technical research council.

- 
- <sup>1</sup>H. Ohnishi, Y. Kondo, and K. Takayanagi, *Nature (London)* **395**, 780 (1998).
- <sup>2</sup>A.I. Yanson, G.R. Bollinger, H.E. van den Brom, N. Agrait, and J.M. van Ruitenbeek, *Nature (London)* **395**, 780 (1998).
- <sup>3</sup>E. Scheer, N. Agrait, J.C. Cuevas, A. Levy Yeyati, B. Ludoph, A. Martín-Rodero, G.R. Bollinger, J.M. van Ruitenbeek, and C. Urbina, *Nature (London)* **394**, 154 (1998).
- <sup>4</sup>M. Brandbyge, M.R. Sørensen, and K.W. Jacobsen, *Phys. Rev. B* **56**, 14 956 (1997).
- <sup>5</sup>J.C. Cuevas, A. Levy Yeyati, and A. Martín-Rodero, *Phys. Rev. Lett.* **80**, 1066 (1998).
- <sup>6</sup>J.C. Cuevas, A. Levy Yeyati, A. Martín-Rodero, G. Rubio Bollinger, C. Untiedt, and N. Agrait, *Phys. Rev. Lett.* **81**, 2990 (1998).
- <sup>7</sup>M. Tsukada, N. Kobayashi, and M. Brandbyge, *Prog. Surf. Sci.* **59**, 245 (1998); N. Kobayashi, M. Brandbyge, and M. Tsukada, *Jpn. J. Appl. Phys., Part 1* **336**, 38 (1999).
- <sup>8</sup>B. Ludoph, M.H. Devoret, D. Esteve, C. Urbina, and J.M. van Ruitenbeek, *Phys. Rev. Lett.* **82**, 1530 (1999).
- <sup>9</sup>M. Brandbyge, J. Schiøtz, M.R. Sørensen, P. Stoltze, K.W. Jacobsen, J.K. Nørskov, L. Olesen, E. Lægsgaard, I. Stensgaard, and F. Besenbacher, *Phys. Rev. B* **52**, 8499 (1995).
- <sup>10</sup>H. Yasuda and A. Sakai, *Phys. Rev. B* **56**, 1069 (1997).
- <sup>11</sup>J.L. Costa-Krämer, N. García, P. García-Mochales, P.A. Serena, M.I. Marqués, and A. Correia, *Phys. Rev. B* **55**, 5416 (1997).
- <sup>12</sup>A. Levy Yeyati, A. Martín-Rodero, and F. Flores, *Phys. Rev. B* **56**, 10 369 (1997).
- <sup>13</sup>P.L. Pernas, A. Martín-Rodero, and F. Flores, *Phys. Rev. B* **41**, R8553 (1990).
- <sup>14</sup>C. Sirvent, J.G. Rodrigo, S. Vieira, L. Jurczyszyn, N. Mingo, and F. Flores, *Phys. Rev. B* **53**, 16 086 (1996).
- <sup>15</sup>N.D. Lang, *Phys. Rev. B* **52**, 5335 (1995); **55**, 4113 (1997); N.D. Lang and Ph. Avouris, *Phys. Rev. Lett.* **81**, 3515 (1998).
- <sup>16</sup>J-L. Mozos, C.C. Wan, G. Taraschi, J. Wang, and H. Guo, *Phys. Rev. B* **56**, R4351 (1997).
- <sup>17</sup>N.D. Lang, *Phys. Rev. B* **55**, 9364 (1997).
- <sup>18</sup>M.J. McLennan, Y. Lee, and S. Datta, *Phys. Rev. B* **43**, 13 846 (1991).
- <sup>19</sup>A-P. Jauho, N.S. Wingreen, and Y. Meir, *Phys. Rev. B* **50**, 5528 (1994).
- <sup>20</sup>M. J. Mehl and D. A. Papaconstantopoulos, in *Computational Materials Science*, edited by C. Fong (World Scientific, Singapore, 1998); M.J. Mehl and D.A. Papaconstantopoulos, *Phys. Rev. B* **54**, 4519 (1996); Parametrization notes can be found at <http://cst-www.nrl.navy.mil>, and parameters for gold at [http://cst-www.nrl.navy.mil/bind/au\\_par\\_99](http://cst-www.nrl.navy.mil/bind/au_par_99)
- <sup>21</sup>P.O. Löwdin, *Sov. J. Chem. Phys.* **18**, 365 (1950).
- <sup>22</sup>Schrödinger's equation in the nonorthogonal basis,  $\mathbf{H}\psi = \epsilon\mathbf{S}\psi$ , is transformed into the usual orthogonal version,  $(\mathbf{S}^{-1/2}\mathbf{H}\mathbf{S}^{-1/2})(\mathbf{S}^{1/2}\psi) = \epsilon(\mathbf{S}^{1/2}\psi)$ , where we identify  $\mathbf{H}_O = \mathbf{S}^{-1/2}\mathbf{H}\mathbf{S}^{-1/2}$ .
- <sup>23</sup>E. Emberly and G. Kirczenow, *Phys. Rev. Lett.* **81**, 5205 (1998).
- <sup>24</sup>In the calculation of the self-consistent potential we use a finite broadening equal to the energy grid spacing ( $>16$  meV) in order to describe the LDOS of the quite localized states ( $d_{xy}, d_{x^2-y^2}$ ) in the narrow contact part. Figure 4 does not include this broadening.
- <sup>25</sup>M. Büttiker, Y. Imry, R. Landauer, and S. Pinhas, *Phys. Rev. B* **31**, 6207 (1985).
- <sup>26</sup>Th. Martin and R. Landauer, *Phys. Rev. B* **45**, 1742 (1992). The unitary matrices  $U_{L/R}$  can be found by diagonalizing  $\mathbf{t}^\dagger\mathbf{t}$  and  $\mathbf{t}\mathbf{t}^\dagger$ .
- <sup>27</sup>M. Brandbyge and M. Tsukada, *Phys. Rev. B* **57**, R15 088 (1998).
- <sup>28</sup>R. Dashen, S-K. Ma, and H.J. Bernstein, *Phys. Rev.* **187**, 345 (1969).
- <sup>29</sup>A.R. Williams, P.J. Feibelman, and N.D. Lang, *Phys. Rev. B* **26**, 5433 (1982).
- <sup>30</sup>M.R. Sørensen, M. Brandbyge, and K.W. Jacobsen, *Phys. Rev. B* **57**, 3283 (1998).
- <sup>31</sup>A. García-Martín, T. López-Ciudad, J.A. Torres, A.J. Caamaño, J.I. Pascual, and J.J. Saenz, *Ultramicroscopy* **73**, 199 (1998).
- <sup>32</sup>J.A. Torres, E. Tosatti, A. Dal Corso, F. Ercolessi, J.J. Kohanoff, F.D. Di Tolla, and J.M. Soler, *Surf. Sci. Lett.* **426**, L441 (1999).
- <sup>33</sup>M. Jonson, I.V. Krive, P. Sandström, and R.I. Shekhter, *Superlattices Microstruct.* **23**, 957 (1998).
- <sup>34</sup>Y. Kawahito, H. Kasai, H. Nakanishi, and A. Okiji, *Surf. Sci.* **409**, L709 (1998).